Proceedings of the 7th International Symposium on Cavitation
CAV2009 – Paper No. 30
August 17-22, 2009, Nobuhiro Hasuike, Michigan, USA

NUMERICAL STUDY ON CAVITATION EROSION RISK OF MARINE PROPELLERS OPERATING IN WAKE FLOW

Nobuhiro Hasuike, Nakashima Propeller, Co., Ltd., Okayama, JAPAN
Shosaburo Yamasaki, Nakashima Propeller, Co., Ltd., Okayama, JAPAN
Jun Ando, Faculty of Engineering, Kyushu University, Fukuoka, JAPAN

ABSTRACT

This paper discusses the application of the CFD to cavitating flow around marine propellers operating in ship wake. Especially the emphasis was put on the tip vortex cavitation and the erosive cavitation around the trailing edge.

This research found that adaptive mesh refinement methodology was effective for the resolution of tip vortex cavitation. Next, barotropy model and full cavitation model were validated, and show qualitatively agreement with the experimental results.

Finally, simple four cavitation erosion indexes were applied for the estimation of the erosion risk and one index shows good agreement with the experimental results. It is concluded that the RANS CFD gives the valuable information for judging the erosion risk although its presumption accuracy and numerical stability need to be improved.

INTRODUCTION

Marine propellers are operating in the unsteady ship wake flow, which causes the repeat of cavitation occurrence and disappearance. Such cavitation causes the serious vibration and erosion problems. Therefore, the decrease of the erosion risk is one of the very important issues in the propeller design. It is necessary to observe the process of cavitation disappearance when the propeller blade moves from high wake region to low wake region for the evaluation of the erosion risk. Especially, latest propellers are designed with skew, and the cavitation erosion may often occur around the trailing edge in larger than 90% radius. Therefore, it is important to observe both blade cavitation and tip vortex cavitation near the very local tip region for the evaluation of the erosion risk.

Recently, RANS method becomes the common useful design tool for the analysis of the flow field around marine propellers, and the application to the cavitation simulation is highly expected.

The RANS simulation becomes an effective method for the evaluation of the erosion risk, if it may simulate the blade cavitation and the tip vortex cavitation in detail. Since cavitation is multi-scale phenomena in time and space, the direct numerical simulation is unrealistic from the limitation of the computing environment. Therefore some simple cavitation models are presented for the general practicable application.

In this research, the propeller cavitation simulations in the wake flow field were performed by using the barotropy model and full cavitation model, and simple practical evaluation indexes for erosion risk were presented.

First of all, numerical simulation of the tip vortex of the DTMB P4119 propeller (Jessup 1989) in non-cavitating condition was performed in order to examine the effectiveness of the adaptive mesh generation. Numerical results of flow field behind the propeller were compared with LDV measurement results. Next, simulations for Seiun-Maru HSP&CP of the non-cavitating and cavitating condition were performed and the pressure distributions and cavitation pattern were compared with the experiments. Finally, by using the above-mentioned strategy of analysis, cavitation simulations were performed for the several kinds of propellers with a different erosion risk. Numerical results were compared with the high-speed video observation results and the simple practical evaluation indexes for erosion risk were validated.

NUMERICAL MODEL

The authors have simulated the flow field around a propeller in both uniform and non-uniform wake using a commercial CFD code. In this research, cavitation on the propeller was simulated using SOFTWARE CRADLE SCRYU/Tetra V7 software, which was based on a finite volume method with an unstructured grid and supports various turbulence models. The k-ε model and the Shear-Stress Transport k-ω model were applied to the present simulations.

Barotropy model

The cavitation model used in this simulation was a barotropic model (e.g., Okuda & Ikohagi 1996) included in SCRYU/Tetra V7. The equation of state for ideal gas

and for pure liquid, which proposed by Tammann, were applied to the gas phase and to the liquid phase, respectively. This equation is approximated by a linear expression of temperature. P_C and T_0 are the pressure and temperature constants of liquid, and K is the liquid constant. These values are estimated by water property. R_g is the gas constant. The gas-liquid two-phase medium inside the cavity is treated as a locally homogenous pseudo-single-phase medium with finite void ratio. The mixture density of a two-phase medium ρ is expressed by the linear combination with the local void fraction (volume fraction) of liquid phase density and gas-phase density with the assumption of a locally homogenous pseudo-single-phase medium. If the pressure P and temperature T of gas and liquid phase are in equilibrium, the equation of state for a locally homogenous pseudo-single-phase medium is given by using the mass fraction of gas phase f in equation (1) as below.

$$\rho = \frac{P(P+P_c)}{K(1-f)P(T+T_0)+R_g f(P+P_c)T} \qquad (1)$$

Full cavitation model (Singhal et al. 2002)

The cavitation model accounts for all first-order effects, i.e., phase change, bubble dynamics, turbulent pressure fluctuations and non-condensable gases contained in the liquid. The basic approach consists of using the standard viscous flow (Navier-Stokes) equations for variable fluid density and a conventional turblence model (e.g., the k-ε model). The fluid density is a function of vapor mass fraction f, which is computed by solving a transport equation coupled with the mass and momentum conservation equations. Suffixes *v*, *g*, *l* denote the vapor phase, non-condensable gass (NCG in short), liquid respectively. $\vec{v}$ is velocity vector. γ is diffusion coefficient of the vapor mass fraction. Net phase change rate is expressed as R_e-R_c. The source terms R_e and R_c denote vapor evaporation and condensation rates. Where, k and σ are the turbulent kinetic energy and the surface tension. The phase change rate R_e and R_c are derived from the Rayleigh-Plesset equation and limiting bubble size (interface surface area per unit volume of vapor) is considered. The evaporation and condensation rates are functions of the instantaneous, local static pressure and kinetic energy are given by:

Using Eqs. (4), (5) and ignoring the second-order derivative, numerical robustness is considerably high, when the bubble propagation and condensation speed is too high. C_e and C_c are the empirical components. It is assumed that saturated vapor pressure P_v depends on the turbulence kinetic energy. ((6), (7)) Subscripts *turb* denotes the turbulence.

$$\frac{1}{\rho} = \frac{f_v}{\rho_v} + \frac{f_g}{\rho_g} + \frac{1-f_v-f_g}{\rho_l} \qquad (2)$$

$$\frac{\partial}{\partial t}(\rho f) + \nabla \bullet (\rho \vec{v} f) = \nabla \bullet (\gamma \nabla f) + R_e - R_c \qquad (3)$$

$$R_e = C_e \frac{\sqrt{k}}{\sigma} \rho_l \rho_v \sqrt{\frac{2(p_v - p)}{3\rho_l}} (1 - f_v - f_g) \qquad (4)$$

$$R_c = C_c \frac{\sqrt{k}}{\sigma} \rho_l \rho_l \sqrt{\frac{2(p - p_v)}{3\rho_l}} f_v \qquad (5)$$

$$P_v = (P_{sat} + P'_{turb}/2) \qquad (6)$$

$$P'_{turb} = 0.39\rho k \qquad (7)$$

COMPUTING SYSTEM

The propeller cavitation simulation in the wake needs wide computational domain that consists of all bladed models. In addition, it is an unsteady calculation therefore it needs a lot of cycles. It also has to reduce time steps from the point of the computational stability compared with the states of non-cavitation simulation. Therefore a huge calculation is needed. In this research, the parallel computing system of 32 nodes (256 cores) based on Windows HPC Server 2008 was constructed for the calculation speed improvement. This system is composed of the calculation nodes (DELL Power Edge1950III, CPU Intel company Xeon, X5460) and Infiniband (Voltaire ISR9024D) for the MPI communication among calculation nodes.

The unsteady calculation of 8000 cycles per about eight million elements can be executed in 20 hours in the calculation that uses 96 cores of this system.

DTMB P4119 PROPELLER

DTMB P4119 propeller, which experimental dataset was used as 22nd ITTC benchmark of RANS calculations, was selected in this research. Table 1 and Fig.1 show the principal particulars and propeller shape. It is valuable for the validation of the presumption of the downstream including the tip vortex because the experimental dataset contains LDV measurement results of downstream of the operating propeller. The presumption accuracy of pressure distribution on the blade and the resolution of the tip vortex become especially important for the detailed cavitation simulation that judge whether the cavitation on the blade side is superior or tip vortex cavitation is superior.

Computational domain

The computational domain is composed of the inner rotational part including the propeller and the outer stationary part. The stationary part and the rotational part are connected discontinuously. Constant velocity and zero pressure are prescribed at the inlet and the outlet boundary, respectively. Fig.2 shows the computational domain. The numerical mesh is an unstructured grid, and basic cells are tetrahedral and prismatic cells are applied to near the blade surface for resolving the boundary layer. First of all, the computational domain was investigated systematically. The SST k-ω model was used for the calculation. It was confirmed that the sidewall influence

was able to be disregarded if approximate 5D was taken for the radius of the outside stationary part. It was confirmed to be able to disregard the influence on thrust coefficient KT if 3D or more was taken from the propeller center to the inlet. Moreover, it was confirmed to be able to disregard the influence in 5D or more about the outlet.

Figs.3, 4 and 5 show these results. Concluding from these results, the radius of the outer stationary cylinder was assumed to be 5D and the upstream boundary was assumed to be more than 3D from the propeller center and the propeller downstream boundary was assumed to be 7D from the propeller center.

Table 1 Principal Particulars of DTMB P4119 Propeller

	DTMB P4119
Number of Blades	3
Diameter(m)	0.3048
Pitch Ratio(at 0.7R)	1.084
Skew Angle(deg.)	0

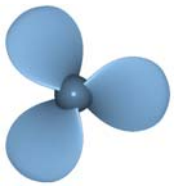

Fig.1 DTMB P4119 Propeller

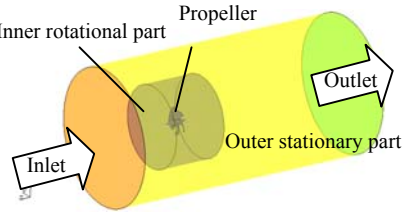

Fig.2 Volume Mesh Region

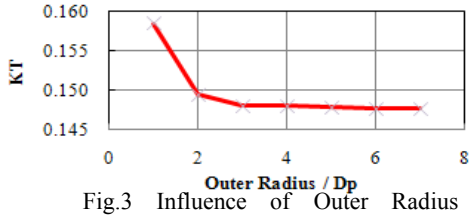

Fig.3 Influence of Outer Radius of Stationary Part on KT

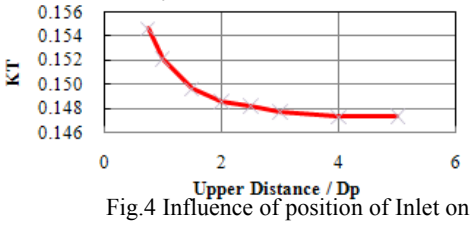

Fig.4 Influence of position of Inlet on KT

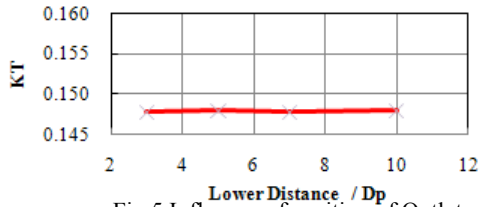

Fig.5 Influence of position of Outlet on KT

Resolution of boundary layer and turbulence model

The arrangement of the prism layer for the boundary layer resolution was examined. The recommended first layer thickness of the prism layer is different by the turbulence model used in the calculation. A standard k-ε model and the SST k-ω model were selected as a turbulence model in this research. The first layer thickness of the prism layer was set to a non-dimensional wall distance for a wall-bounded flow (y^+ in short) =1 in the case of the SST k-ω and set to y^+=50 in the case of the k-ε model. The number of layers and the increase rate of thickness of the prism layer were changed. The computational results of the velocity distribution of the inner boundary layer are compared with the experimental results in Figs.6 and 7. Total thicknesses of the prism layers for boundary layer resolution are shown in the figures. The increase ratios of thickness of the prism layer and the turbulence model used in the calculation were shown between parentheses. It was confirmed that the presumption accuracy of the velocity distribution of the inner boundary layer improved if total thickness of the prism layer becoming thicker than approximate 2.3mm. Moreover, it was confirmed that turbulence model effects on the accuracy of the velocity distribution of the inner boundary layer. The k-ε model reproduced comparatively thicker boundary layer when total thickness of the prism layer is thicker than approximate 2.3mm, and shows good agreement with the experimental measurement results shown in figure as "Tripped" which means the state of with roughness on the leading edge of the propeller. The estimated boundary layer thickness by the SST k-ω model was thinner than the experimental measurement results shown in figure as "Smooth" which means the state of without roughness on the leading edge of the propeller.

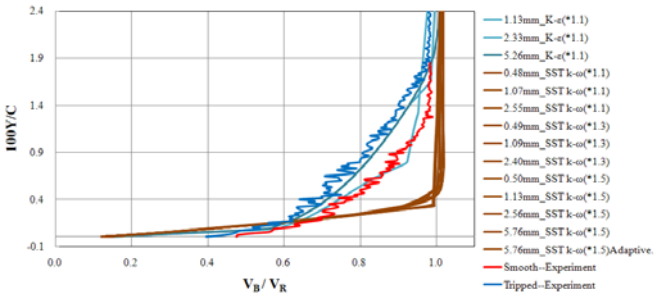

Fig.6 Boundary Layer Profiles at r/R=.7, Suction Side, Xc=0.9

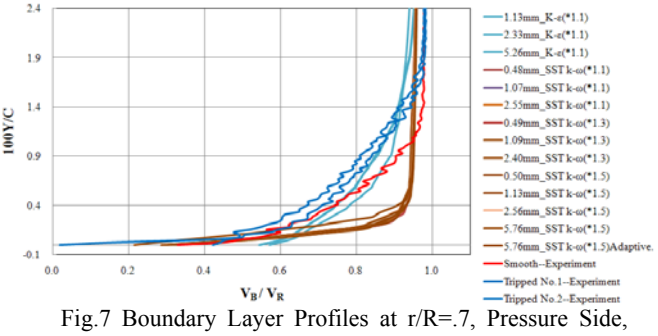

Fig.7 Boundary Layer Profiles at r/R=.7, Pressure Side, Xc=1.0

Propeller open characteristics

The influence on the presumption accuracy of propeller open characteristics (POC in short) by the difference of the turbulence model were examined. In the calculation by using the k-ε model, the first layer thickness of the prism layer was set to y^+=50, and total thickness of the prism layers was 5.26mm. In the case of using the SST k-ω model, first layer thickness of the prism layer was set to y^+=1, and total thickness of the prism layers was 5.76mm. The calculated propeller open characteristics in different operation points are compared with the model test in Fig.8. It is confirmed that calculated KT is smaller than the model test results and KQ is a little larger than the model test results in the overall range of the advance coefficient J in the case of the k-ε model. KT is a little larger than the model test results and KQ is corresponding to the model test results well in the case of the SST k-ω model. It is thought that the k-ε model overestimates a viscous component of the torque and the estimated efficiency becomes lower than the model test. The SST k-ω model shows no overestimation of a viscous component of the torque and propeller efficiency becomes higher than that of the k-ε model. Figs.9 and 10 show the comparative results of pressure distribution at 0.7R and 0.9R. The computational results of both the k-ε and the SST k-ω are corresponding comparatively well with the experimental results.

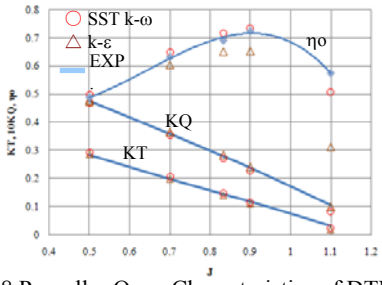

Fig.8 Propeller Open Characteristics of DTMB P4119

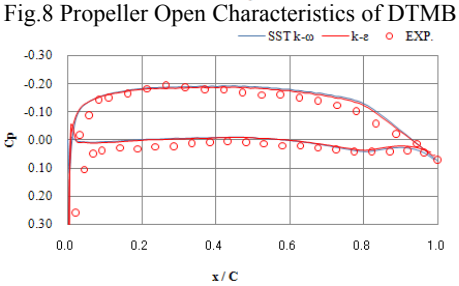

Fig.9 Chordwise Pressure Distributions at r/R=0.7

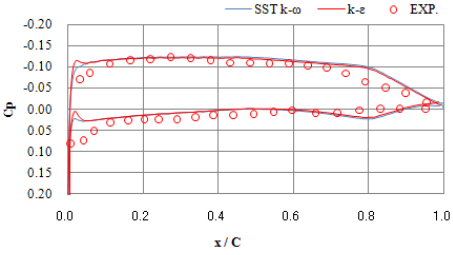

Fig.10 Chordwise Pressure Distributions at r/R=0.9

Velocity distributions downstream of the propeller

The validation of the resolution of the propeller downstream was conducted. The propeller cavitation simulation in the wake needs wide computational domain which consists of all bladed model. And the very fine meshes are required especially for the tip vortex resolution. Therefore a huge number of meshes are needed. As it is important to arrange very fine meshes only at the part of tip vortex for the efficient calculation, the adaptive mesh refinement methodology was examined. Adaptive mesh refinement procedure is as follows:

At first initial flow field is solved with using comparatively coarse meshes. The next mesh is created with refinement at the part of high physical quantity gradient obtained by first calculation and is used as next calculation. These procedures are repeated several times. The adaptive mesh refinement methodology supported by SCRYU/Tetra 7 recreates whole meshes therefore mesh quality is kept comparatively high. Especially for the unsteady cavitation simulation needs robustness of the calculation. Therefore keeping meshes quality high is very effective. In this research, it was confirmed that adaptive mesh refinement by the velocity gradient was effective. Mesh refinement procedure was adapted to the downstream of the one blade. For the priority at the downstream, mesh refinement was not adapted near the blade surface, although pressure and velocity gradient was high near the blade surface. Octants less than 0.3mm used in mesh refinement are shown in Fig.11. Surface meshes near the blade surface and tip vortex are shown in Fig.12. The SST k-ω model and the k-ε model were used in the calculation. Axial velocity downstream of the propeller at 0.7R and at x/R=0.3181 are shown in Fig.13. Fig.14 shows pressure distribution at x/R=0.3281. The boundary layer downstream of the propeller was obtained and low negative pressure at the tip vortex core was confirmed. Axial velocity, tangential velocity and radial velocity were compared with LDV measurements in Figs. 15, 16, 17 and 18. Calculation results at 0.3R show weak velocity gradients by the SST k-ω model. The Calculated results by the k-ε model show good agreement with the experimental results. Calculated velocity distributions of both the SST k-ω model and the k-ε model at 0.7R, 0.9R and 0.924R(through tip vortex) show good agreement with the experimental results, although the some difference of the phase angle is shown in the Figs.

Fig.11 Octants Arrangement(<0.3mm)

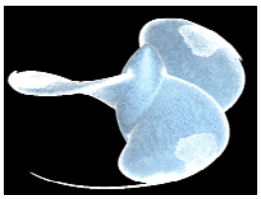

Fig.12 Mesh near the Blade

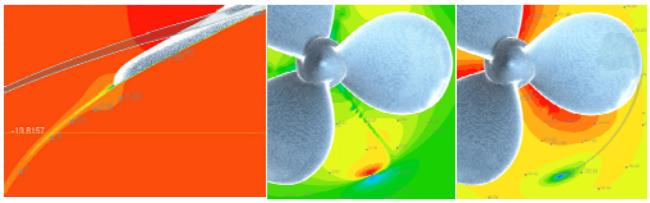

r/R=0.7 X/R=0.3281 X/R=0.3281

Fig.13 Axial Velocity Contour Fig.14 Pressure Contour

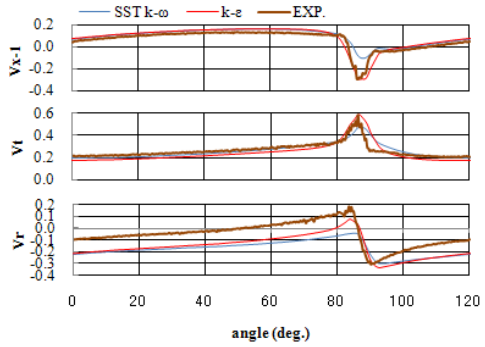

Fig.15 Velocity at X/R=0.3231, r/R=0.3

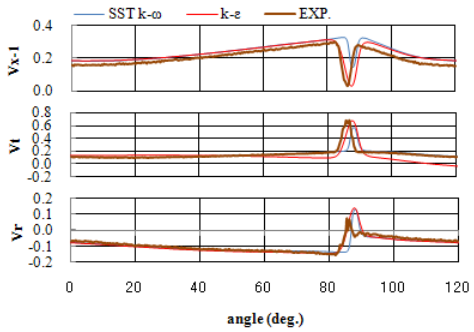

Fig.16 Velocity at X/R=0.3231,

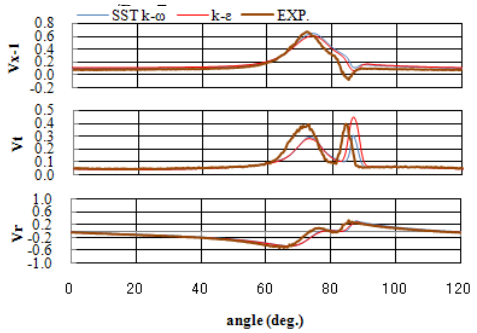

Fig.17 Velocity at X/R=0.3231,

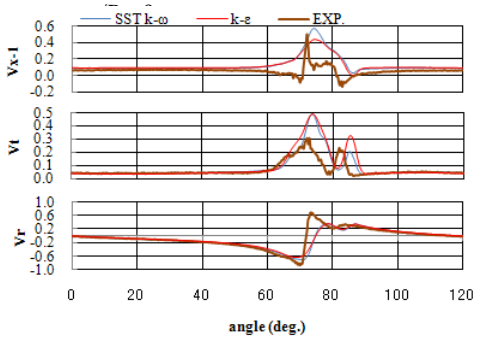

Fig.18 Velocity at X/R=0.3231, r/R=0.924 through Tip Vortex

SEIUN-MARU PROPELLERS

In this research, calculations were conducted with a highly skewed propeller (HSP in short) and a conventional propeller (CP in short) of "Seiun-Maru". These propellers have rich experimental data that contain precious data such as pressure measurement on the blade surface in full scale (Ukon 1990, Ukon 1991, Hoshino 1998) and cavity shapes measurement on the model scale propellers (Kudo 1989, Kurobe 1983). Principal particulars of the propellers and the axial wake distribution are shown in Table 2 and Fig.19. HSP, which has a skew angle of 45º, is known well by being influenced by viscosity more strongly than conventional propellers (Kakugawa 1986), therefore it seems to be appropriate for use in CFD evaluation.

Table 2 Principal Particulars of Seiun-Maru HSP&CP propeller

	HSP		CP
Scale	Actual	Model	
Number of Blades	5		
Diameter(m)	3.6	0.22	0.22095
Pitch Ratio(at 0.7R)	0.944		0.95
Skew Angle(deg.)	45		10.5
Expanded Area Ratio	0.7		0.65

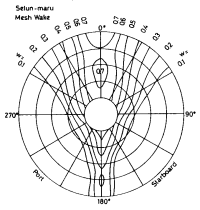

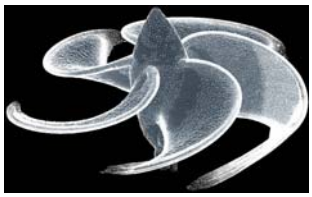

Fig.19 Wake Distribution Fig.20 Mesh near the Blade Surface

Unsteady non-cavitating condition

Full scale HSP, which experimental dataset was used as 22nd ITTC benchmark of RANS calculations, was selected for the validation of unsteady non-cavitating condition. Unsteady calculation in the wake by the CFD should give velocity distribution to the inlet boundary of the propeller upstream. The aim of the present calculation is the unsteady analysis of the cavitation that is the multiscale timewise and spatially, therefore it is necessary to concentrate the meshes near the propeller blades. It was not possible to execute it from the limitation of the computing environment, though the most reasonable method seemed analysis including the hull. In this analysis, the axial wake distribution, the tangential projection, and the radial wake distribution are given as the inlet boundary condition. It needs to keep wake distribution at propeller upstream to accomplish the high presumption accuracy. The inlet boundary was adjusted from the propeller center to the position of 0.7D to remove the influence of decrease of the velocity gradient of the wake. In the propeller open tests, the above-mentioned validation of analysis domain indicates that taking the distance of approximate 3D is necessary to remove the influence of the inlet boundary position to calculate the POC unknown a priori. On the other hand, in the state of unsteady simulation in the wake, the

calculated time-averaged KT is adjusted to already-known KT by adjusting the inlet velocity iteratively, therefore pressure distribution on the blade surface is thought to be almost appropriate. The inlet boundary, the outlet boundary and the radius of the outer stationary cylinder of the outer stationary part were adjusted from the propeller center to the position of 0.7D, 7D and 5D. The adaptive mesh refinement methodology was used for the resolution of tip vortex. To calculate efficiently, the mesh density of one blade out of five blades was enlarged. Fig.20 shows the numerical mesh near the tip vortex. The number of total elements finally generated became about 13 million elements. Calculation was conducted with the k-ε model in full scale.

Numerical results

The pressure fluctuations on the blade at 0.7R and 0.9R are compared with measurement results in full scale and calculation results from Hoshino in Figs.21 and 22. The calculated pressure distributions of 0.7R obtained by this calculation showed approximate agreement with the results from Hoshino. Better agreement at 60% chord position and 80% chord position of 0.7R are obtained, the negative pressure is estimated small at 40% chord position. The calculation results at 0.9R also agree with the calculation results by Hoshino. The low negative pressure at 60% position and 80% position shown in measurement results in full scale were not able to simulated by the calculation. The chordwise pressure distribution at 0.7R and 0.9R with blade rotating position from top of 0deg., 90deg., 180deg. and 270deg. were compared with measurement results in full scale and calculation results from Hoshino in Figs. 23 and 24. The computational results and the measurement results show roughly good agreement at 0.7R and some discrepancies around the trailing edge at 0.9R.

Unsteady cavitating condition

The calculations in the unsteady cavitating condition were validated with the unsteady cavity shape measurements results on HSP and CP by Kudo et al. (1989). The operating conditions were set to the same conditions as the model tests. In the case of HSP: cavitation number σ_n=3.06 and KT=0.207. In the case of CP: σ_n=2.99 and thrust KT=0.201

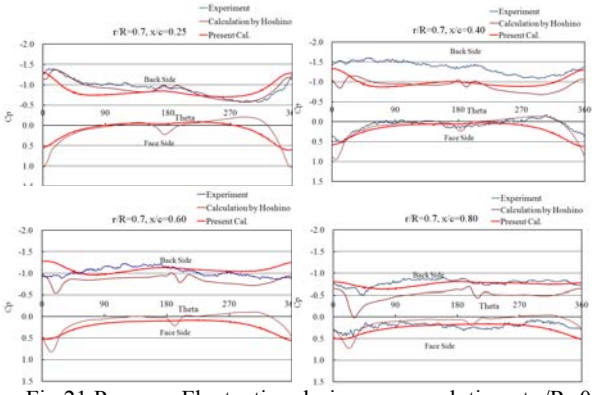

Fig.21 Pressure Fluctuation during one revolution at r/R=0.7

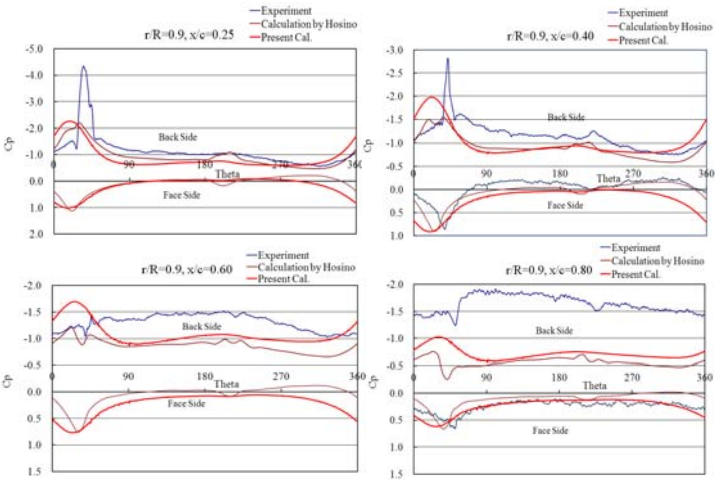

Fig.22 Pressure Fluctuation during one revolution at r/R=0.9

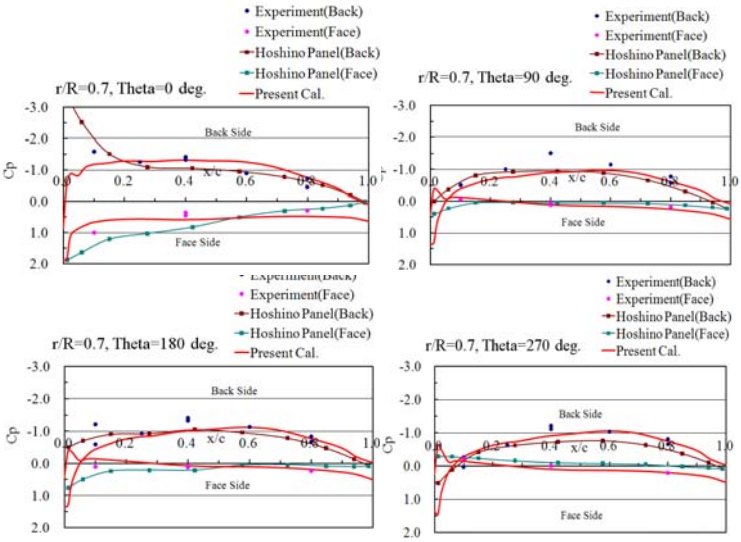

Fig.23 Chordwise Pressure Distribution at r/R=0.7

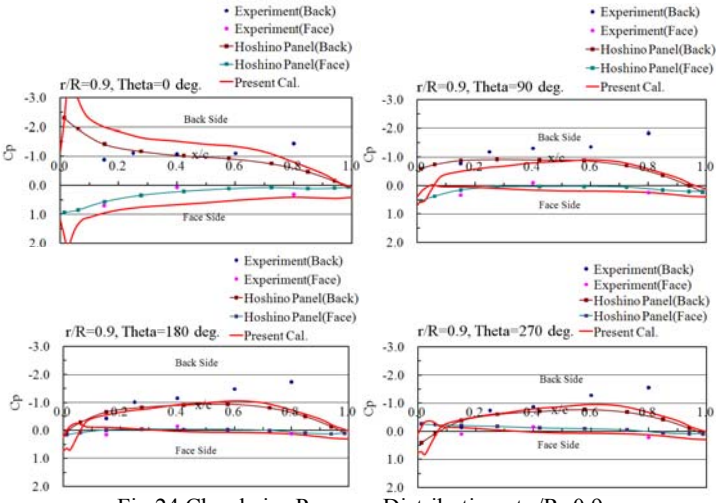

Fig.24 Chordwise Pressure Distribution at r/R=0.9

Numerical background regarding robustness of cavitaiton simulation

Authors conducted the cavitation simulation with the barotropy model for HSP and CP in previous research (Hasuike 2009), and have suffered from the problem of instability of the calculation. The calculation of the

propeller cavitation in the wake often becomes unstable because of the density difference between the gas phase and liquid phase. The factors that influence the computational stability were systematically investigated. The low quality meshes near the blade edges and the advective term accuracy much influenced computational stability. The computational stability was prioritized, therefore the first upwind discretization for the advective term accuracy was used and only one prism layer was arranged for the boundary layer resolution on the blade surface. The calculated cavity void fraction became remarkably low and was thought not to be enough in accuracy. In this research, the factors that influence the accuracy on the cavitation were systematically investigated on 2D aerofoils . It was confirmed that the advective term accuracy and the total thickness of the prism layer near the blade were especially important to improve the accuracy. So much effort was made on mesh quality improvement and selection of more robust combination of a cavitation model and a turbulence model to improve the accuracy of cavitation simulation. Total thicknesses of prism mesh layers arranged near the blade edges were thin for the prevention of decrease of mesh quality. Total thicknesses of prism layers arranged near the blade surface except edges were thick enough for the resolution of the cavitating region. This strategy enabled the stable calculation with comparatively high quality mesh. Fig.25 shows prism mesh layers near the blade surface.

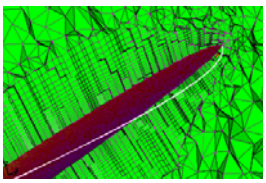

Fig.25 Prism Mesh Arrangement near the Blade Edge

Moreover, the influence of the cavitation model on the computational stability was investigated with barotropy model and Singhal's full cavitation model. Unsteady propeller simulation in the wake uses the sliding mesh methodology, therefore the physical quantity at the discontinuous boundary between the outer stationary part and the inner rotational part are interpolated. As a result, an irrational negative pressure often may occur in the calculation process. In such case, barotropy model showed the unstable behavior caused by the instantaneous phase change between vapour and liquid. The full cavitation model showed comparatively stable behavior because the phase change was comparatively smooth by solving the transport equation of the cavity void fraction and and an unreal cavitation was not generated due to the condensation term at the meshes where accuracy was deteriorated. Moreover, SCRYU/Tetra uses the implicit method in the unsteady calculation and it is necessary to reduce the CFL number. In the case of the SST k-ω model, y^+ should be adjusted to about 1,therefore fine mesh is needed near the blade and time step should be reduced to keep CFL number small. In the case of the k-ε model, y^+ should be adjusted to about 50 and the mesh size is able to be comparatively enlarged, therefore time step is able to be more enlarged than the case of the SST k-ω model to keep CFL number small. Moreover, the k-ε model was superior to the SST k-ω model from the aspect of the computational stability in the case of the combination with the full cavitation model.

After the investigation of the robustness, calculations were conducted in model scale with the k-ε model. It was supposed that it was necessary to calculate the leading edge separation and tip vortex because the model-scale experimental cavitating range of HSP was comparatively few and located in the leading edge and blade tip. The inlet boundary, the outlet boundary and the radius of the outer stationary cylinder of the outer stationary part were adjusted from the propeller center to the position of 0.7D, 7D and 5D. In this analysis, the axial wake distributions are given as an inlet boundary condition. KT was adjusted to already-known KT same as the model test condition. The adaptive mesh refinement methodology was used for the resolution of tip vortex. To calculate efficiently, the mesh density of one blade out of five blades was enlarged. The propeller is rotated 1800deg. by 1deg per cycle to develop flow field, after that 0.15deg. per cycle is adopted during the final time step. The second order accuracy of the advective term was adapted. The barotropy model and the full Cavitation model were used in the calculation. In the case of the barotropy model, the void mass fraction of the vapour of the inlet boundary was assumed to be 0.1%. In the case of full cavitation model, NCG was set to 1ppm and the empirical constants Ce and Cc were set to 0.25 and 0.001 respectively. Ce and Cc was decided from the condition of becoming the cavitating range equal with the barotropy model. The cavitation extent on the blade of HSP is compared with the experimental results in Fig.26. The contour of 2% cavity void fraction was shown in the case of barotropy model and the contour of 3% cavity void fraction was shown in the case of the full cavitation model. Some ranges of the cavitation inception caluculated by both barotropy model and full cavitation model are overestimated comaparing with the experimental results. As for the tip vortex, the angle of rotation increases, it strengthens, the tendency to the model test is reproduced well, and the effectiveness of the solution by adaptive mesh generation can be perceived. Next, the void fraction at 0.9R and 0.95R are compared with the results of the cavity shape measured by Kudo's et al. in Fig.27. Figure shows the void fraction contour from 2% to 100%.

The outer boundary of the colored region was corresponding to 2% of void fraction. The contour line was arranged at intervals of 5% of the cavity void fraction. The contour lines of the void fraction of 2% of both the barotropy model and the full cavitation model show a good agreement with the experimental results by Kudo et al. at 0.9R and 0.95R except the extremely thick cavitation closure around the trailing edge. The contour is very dense in the vertical direction of the blade, therefore

any contour lines more than 2% may roughly agree with the experimental measurements. Moreover, regarding the chord-wise extent of cavitation, cavity void fraction was high at 20 deg. on the development process from the leading edge toward the trailing edge. The intervals of contour of the cavity void fraction of 2% and 7% were wide and cavity closure was not able to be decided clearly. The intervals of the contour of the void fraction of 2% and 7% calculated by the full cavitation model were wider than that of the barotropy model. It was thought that the generated cavitation was hard to condense by using C_c=0.001 smaller than suggested constant C_c=0.01 in the case of full cavitation model. Moreover, calculated cavity void fraction of 0.9R on the condensation process of the cavitation more than 20deg from the top was comparatively low.

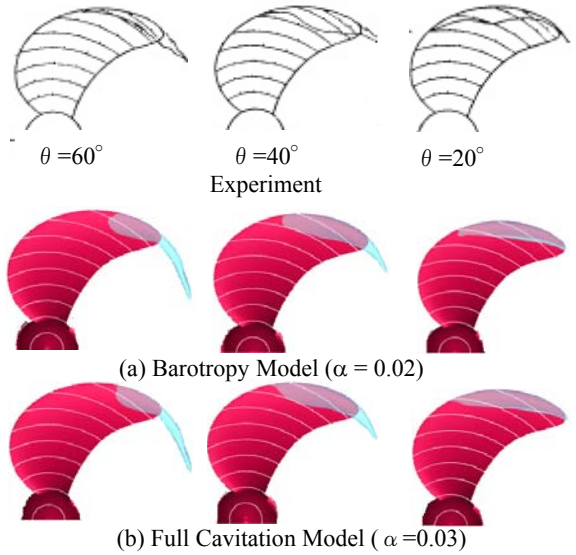

Fig.26 Cavitation Extent on HSP

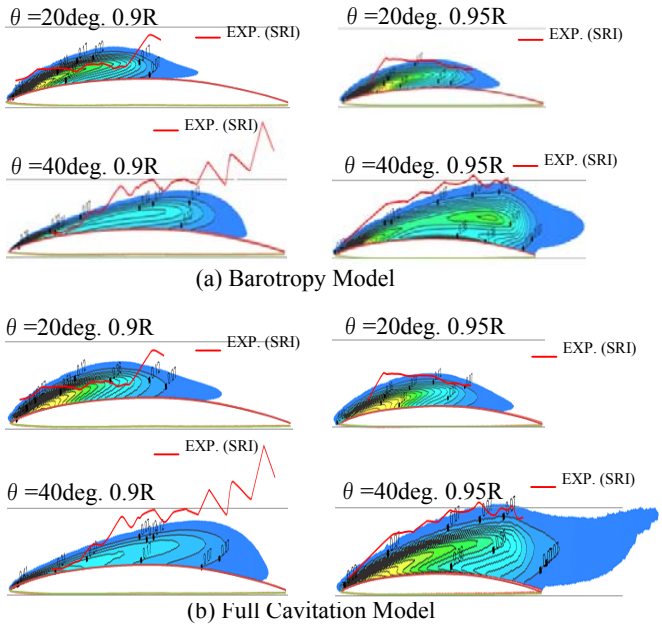

Fig.27 Comparison between Measured Cavity Sections and Calculated Contours of Cavity Void Fraction on HSP

Therefore it is thought to be necessary to pay attention to the contour of a comparatively small void fraction to estimate the condensation process of the cavitation. In this research, it was not able to confirm which cavitation model was better in view of the accuracy. Calculated results of CP were obtained only by the full cavitation model. The cavitation extent on the blade of CP is compared with the experimental results in Fig.28. The contour of 3% cavity void fraction was shown in (a) and the contour of 10% cavity void fraction was shown in (b). In the case of CP, the range of the calculated contour of cavity void fraction of 3% is larger than cavity extent of the experimental results. The range of the calculated contour of cavity void fraction of 10% is almost corresponding to the experimental results. Next, the void fractions at 0.9R and 0.95R were compared with the results of the cavity shape measured by Kudo et al. (1989) in Fig.29. The contour line of the void fraction of 2% shows a good agreement with the experimental results by Kudo et al. (1989) at 0.9R and 0.95R except for the extremely thick cavitatin closure around the trailing edge. Moreover, about the chord-wise extent of cavitation, cavity void fraction was higher than that of HSP at the mid chord. The intervals of contour of the void fraction from 2% to 7% were wider than that of HSP.

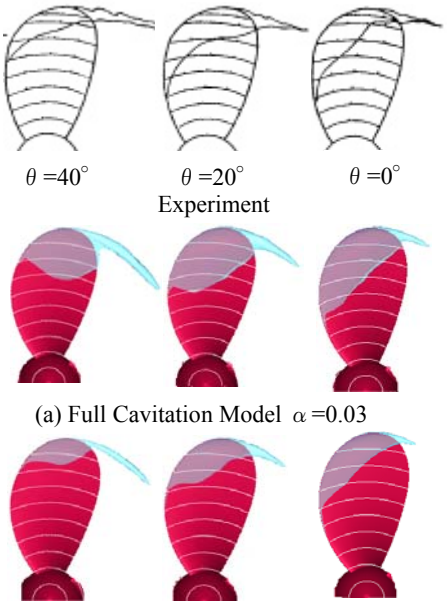

Fig.28 Cavitation Extent on CP

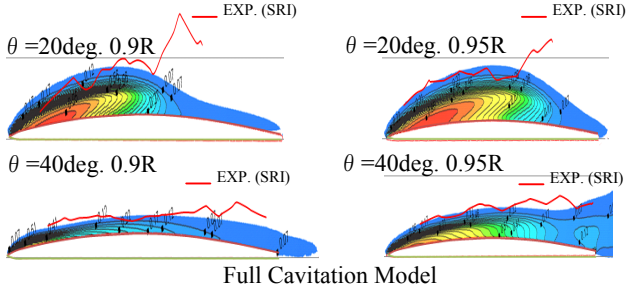

Fig.29 Comparison between Measured Cavity Sections and Calculated Contours of Cavity Void Fraction on CP

In this research the cavity void fraction used for the comparison with the model-scale experimental were 2-3% in case of HSP and 10% in case of CP. CP was compared with experimental results with 10% contour same as Kawamura et al. (2009) although the possibility of underestimating cavitating region was pointed by Kawamura et al. in their research. There is a possibility that this calculation also underestimating the cavity void fraction. The void fraction used for the comparison by the VIRTUE project of the EU (Salvatore 2009) was 50%, and roughly good agreement was shown in the cavitation calculation in a steady cavitating condition. Generally, σ is small, and it is a leading edge cavitation fixed to the leading edge, and cavity closure position may not greatly change in a model test in the uniform flow. In such case, the contour of the void fraction in the rear end of the cavity is dense, and comparatively suitable for the model test in a high void fraction is expected. In VIRTUE, the comparison in the wake flow was also conducted with the contour of the void fraction 50%. It was a comparison of the testing conditions limited to the cavitation fixed within the very little range of the leading edge. The advection of the cavity is thought in the testing condition described in the later chapter, and cavitation is not always the fixed cavitation.

And the cavity void fraction of cloudy cavitation is thought to be comparatively low. In such case, the comparison with 50% contour of the cavity void fraction is thought to be mismatch.

The room for argument remains to what value of cavity void ratio should be used for the comparison with the model experiment.

The example of applying the calculation of the cavitating propeller in the wake is expected, and the measurement result of the pressure distribution on the cavitating blade in the wake is also expected.

VARIOUS LOAD DISTRIBUTION PROPELLER

Model test of propellers having various load distributions near the blade tips.

Recently the authors have found that tip loaded propellers offered better results against cavitation erosion in several model tests on small blade area propellers aiming at increase in the efficiency. In this paper, four types of propellers were designed for the container vessel with the tip load distribution varied systematically to examine the reason why the tip loaded propeller was more effective against cavitation problems than the commonly used tip unloaded one and to find the design criteria on the prevention against cavitation erosion.

In order to investigate the relation between the tip load distribution and the cavitation performance with high cost effectiveness, four-bladed propeller model whose individual blades have different tip load distributions was used for the cavitation tests. This special propeller model is very effective to perform cavitation tests with less experimental uncertainty due to water quality in a cavitation tunnel. This experimental technique was applied for cavitation tests, (e.g., Takahashi 1959, Ukon 1981). By using the present models in the cavitation tests, cavitation patterns on four kinds of blades can be observed during one test run and evaluated cavitation characteristics on each blade easily. On the other hand, small influence on cavitation due to the interference from the neighboring different blades cannot be avoided, not as that of the propeller with all the blades of the same shape.

Table 3 shows the propeller principal particulars and Fig. 30 shows the hull wake pattern of the containership. Fig.31 shows the photograph of the model propeller. The right side of figure is shown referring to the propeller of the development area ratio generally adopted by this design condition. The left side of the Figure shows propeller used in this research. The blade area ratio was 20% smaller than ordinary design propeller aiming at higher propeller efficiency. Fig. 32 shows the comparison of the radial pitch distribution among these propellers. Each blade of the four-bladed propeller model can be specified by single alphabetical character after the propeller number, namely A, B, C, D. All blades of propeller were designed by keeping the thrust coefficient KT 0.15 for the design point and by systematically varying the blade tip load from heavily loaded to lightly loaded distributions using the LST for a container ship. Fig. 33 shows the circulation distribution of the propeller working in the averaged wake of this containership at the design condition. They are estimated by the LST, (e.g., Yamasaki 1981). All of the circulation distribution curves of four blades cross at the location slightly below 0.8R due to the design constraint to generate the same thrust under the various blade tip loadings. The heavier the blade load near the tip becomes, the larger the circulation near the tip and in contrast the smaller that near the boss become.

Cavitation Observation

The thrust coefficient K_T of the propeller and the cavitation number σ_n for the high-speed video observation was set to 0.161 and 1.7 respectively. Figs. 34 and 35 are the series of representative flames of cavitation taken by the high-speed video camera. Figs .34 and 35 indicate the process from the cavitation inception to the collapse of sheet cavity on blade (A) and (D). Analyzing from these photographs and the animations of a high-speed video camera, the cavitation behaviors on each blade can be summarized as follows.

The extent of blade surface cavitation on blade (D) (the most lightly loaded propeller) was the largest and the collapsing time of the sheet cavity was the shortest. When the size of the sheet cavitation on the blade reached the maximum, it extended from around 0.5R to the tip and then flowed toward the trailing edge with the cavity interface partially collapsing into small cavity bubble clusters. The rapidest collapsing and rebound were observed around the trailing edge from 0.7R to the tip during the final collapsing stages of the sheet cavitation.

Immediately after the cavity collapsed, the intense flash from the collapsing cavity was found in the wide area from the tip towards the root. The blade surface cavitation on the blade (A) and (B) (the moderately tip loaded propellers) extended to the relatively limited region around the tip and collapsed gradually, compared with that on the blade (D), i.e., lightly tip loaded one. The cavitation of the blade (A) and (B) developed along the leading edge between 0.65R and 0.7R during the inception stage. The blade surface cavity grew and spread over the blade between 0.65 and 0.7R to the tip. The cavity collapsed around the trailing edge from 0.85 to the tip with slower speed than that in the lightly tip loaded case. The collapsing cavity was involved into the tip vortex cavitation and shed downstream. Fig.36 shows the state of blade surface of the suction side of blades (A), (B), (C) and (D) after the series of cavitation experiments. The blades of (A) and (B) had no damage and were expected to be used without serious risk of cavitation erosion. By contrast, the black lines drawn by a maker pen around the trailing edge at 0.9R and 0.95R of the blade (C) was removed off. In the extreme case, such as the blade (D), the trailing edge at 0.95R chipped off and the lines at 0.9R and 0.95R were removed off. The trailing edge was slightly bent to the pressure side of the trailing edge at 0.88R. No damage indicating erosion risk was found around the trailing edge between 0.7R and 0.8R where the rapid collapse of sheet cavity was observed. According to the results from the present experiments, it is concluded that the sheet cavitation on the heavily tip loaded blades occurs limitedly around the tip and the cavity collapse is delayed until it is involved into the tip vortex cavitation. By contrast, the cavity on the lightly tip loaded blades tends to collapse on the blade surface and has more risk to cause cavitation erosion than that on the heavily tip loaded blades.

Table 3 Principal Particulars of MPNO.1

	MPNO. 1			
	A	B	C	D
Number of Blades	4			
Diameter(m)	8.2			
Pitch Ratio(at 0.7R)	1.026	1.051	1.077	1.105
Skew Angle(deg.)	30			
Expanded Area Ratio	0.52			

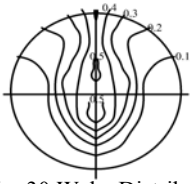

Fig. 30 Wake Distribution

MPNO.1

For reference

Fig. 31 Model Propeller

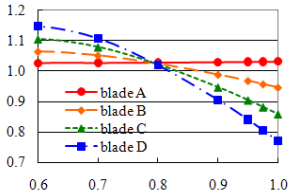

Fig. 32 Pitch Distribution

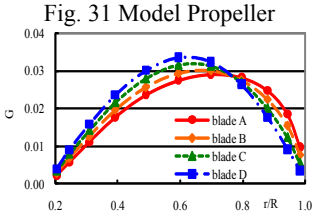

Fig. 33 Circulation Distribution

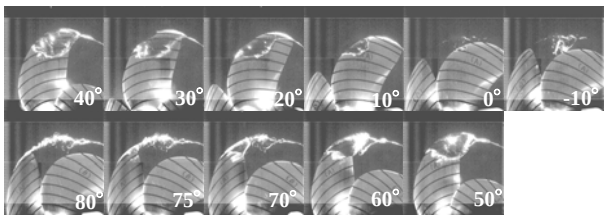

Fig.34 Cavitation on Blade(A)

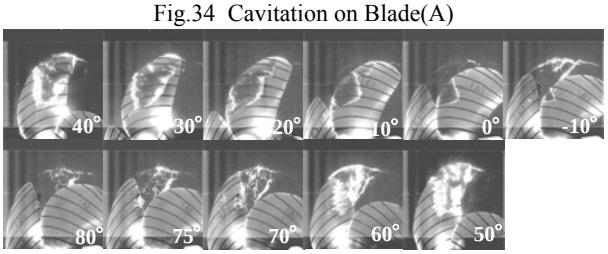

Fig.35 Cavitation on Blade(D)

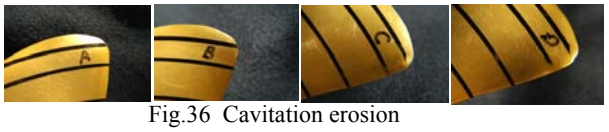

Fig.36 Cavitation erosion

Cavitation simulation

The computational domain is composed of the inner rotational part including the propeller and the outer stationary part. As for the blade part, the shape of each blade was different as well as the model propeller. The numerical mesh was an unstructured grid, and basic cells are tetrahedral and prismatic cells were applied to near the blade surface for resolving the boundary layer.

The inlet boundary, the outlet boundary and the radius of the outer stationary cylinder of the outer stationary part were adjusted from the propeller center to the position of 0.7D, 7D and 5D. The k-ε model was used for the calculation. The adaptive mesh refinement methodology was used for the resolution of tip vortex. The number of total elements finally generated became about 20 million elements. The propeller was rotated 1800deg. by 1deg per cycle to develop flow field, after that 0.15deg. per cycle is adopted during the final time step. The second order accuracy of the advective term was adapted. The full Cavitation model was used in the calculation. NCG was set to 1ppm and the empirical constants C_e and C_c were set to 0.25 and 0.001 respectively. As for the blade (D) where erosion was caused, the attack angle was small near the tip, on the other hand the attack angle was large from 0.6R to 0.8R. Therefore the cavitation inception was occurred at comparatively small radius. After the range of the cavitation expands, erosion was caused through the process that the cavitation remained like a patch around the trailing edge. When the cavitation remains like a patch on the blade immediately before condensation, it is thought that the erosion is easy to occur. The attack angles from 0.6R to 0.8R were comparatively large, therefore the remained cavitation around the trailing edge was not thought to be caused by a low negative pressure at the mid chord. The cavitation, where occurred near the leading edge at comparatively small radius, continued to remain and advect from the leading edge to the trailing

edge on the space without disappearing easily, although the negative pressure become higher than the vapour saturated pressure. The cavitation in such a disappearance stage corresponds to the part of closure of the cavity, the cavity void fraction has become comparatively lower, and the cavity closure boundary was thought to be unclear. Therefore, the visualization that pays attention on the contour of a comparatively low void fraction ratio is thought to be effective to estimate the process where such a cavitation disappears. Then, the contour of the cavity void fraction 2% was used for the comparison in this research. Fig.37 shows the computational results. The tip vortex cavitation was strong, and the cavitation disappears comparatively smoothly from the boss side toward the tip side in the radial direction. On the other hand, the tip vortex was weak, and the cavitation region at the mid radius was large on the D blade. When the cavitation disappears after the rotating position of 60 deg., the thick cavity was observed in the trailing edge like a patch. Such a cavity pattern suggests the risk of cavitation erosion. These computational results reasonably correspond to the experimental results. The RANS computations agree well with the experimental results qualitatively.

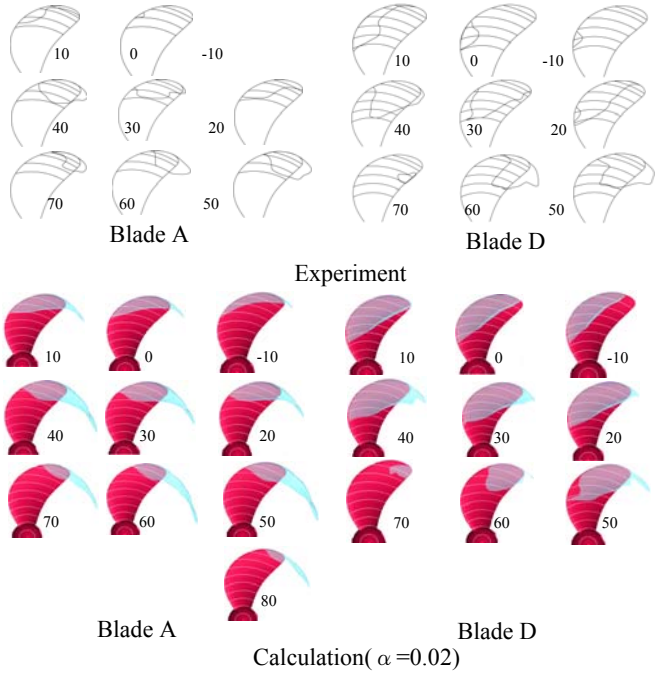

Fig. 37 Cavitation Extent

Numerical simulation of the cavitation erosion risk

It is thought that cavitation erosion is a fatigue phenomenon caused by the impact load generated when the cavitation bubble collapses acts repeatedly on the solid surface in neighborhood.

Nowadays, the generation of such an impact load is predictable in the three-dimensional numerical analysis in the state of the single bubble. However, when the many bubbles collapse, calculating the phenomenon of the load acting on the surface of the fluid machinery in three dimensions in detail is difficult in current computer ability. Therefore, it is thought to be practicable that the physical index obtained from the global flow analysis is related to the strength of cavitation erosion. Nohmi et al. (2008) conducted the analysis of cavitating hydrofoil by the barotropy model in combination with the bubble dynamics, and it was confirmed that the pressure of the bubble advecting in the flow field might oscillate when ambient pressure rises. It was also confirmed that the inner pressure of the bubble is extremely higher than ambient pressure and cause the danger of cavitation erosion. Nohmi et al. (2008) suggested the simple indexes related the strength of cavitation erosion from their finding. These indexes were applied to the three-dimensional unsteady cavitation analysis of the propeller in this research, and the evaluation of the erosion risk is tried. The indexes are shown in expressions (8) - (11). It is expected to be quantitative comparison of erosion risk of a different blade although there is no physical meaning in the absolute value of the indexes. Expressions (8) - (11) are shown by the product of the numerical value of the cavity void fraction or time differential of cavity void fraction at the surface position and the pressure recovery or time differential of pressure. Each expression assumes that erosion may easily occur when the cavity void fraction is high or the level of the pressure recovery is large.

$$Index1 = \alpha \bullet \max\left[\frac{\partial p}{\partial t},0\right] \quad (8)$$

$$Index2 = \alpha \bullet \max[(p - p_v),0] \quad (9)$$

$$Index3 = \max\left[-\frac{\partial \alpha}{\partial t},0\right] \quad (10)$$

$$Index4 = \max[(p - p_v),0] \bullet \max\left[-\frac{\partial \alpha}{\partial t},0\right] \quad (11)$$

Figs.38 and 39 show the computational results and high speed measurements of the rotation angle from 50deg. to 70deg. The part with large value of index is shown in red in Fig.38. Each index value becomes the greatest value immediately before the disappearing of the cavitation. This tendency is correspond to the experimental results and appropriate. The tip vortex cavitaion on the blade (A) is strong in the wide range of the rotating direction by tip loading and the negative pressure in the tip vortex is constant and stable. Therefore, each erosion index becomes $_{P=P_v,\partial\alpha/\partial t=0}$ and it is presumed that the risk of erosion is low in the tip vortex. Some index values around the trailing edge at the inner radial position of the tip vortex are growing from 0.95R to 0.975R. This location is corresponding to the position of erosion often seen with a recent high skew propeller. The part with a large index smoothly moves to a tip side along with the cavitation disappearing toward the blade tip. The indexes values of the blade (A) are smaller than those of the blade (D), and the erosion risk of the blade (A) is presumed to be smaller than that of the blade (D). This tendency agrees with the experimental results. The indexes contours show some

differences. Indexes 1, 3, and 4 are the patterns that look like very well. But these index values at the mid chord of 0.95R at 70deg. are greater than index values around the trailing edge of 0.95R at 65deg. In the model test, rapidly collapse of the cavitation at trailing edge from 0.9R to 0.95R was observed. Index 1,3 and 4 disagree to the position in which erosion was caused in the model test. The contour of Index2 is dividing into two parts at 65 deg. One is located around the trailing edge from 0.9R to 0.95R and the other is located at blade tip. Rapid shrinkage occurred at 65 deg. in the model test and the tendency is corresponding well. In the model test, the rapid shrinkage of tip vortex was observed, and it was observed that cavitation like patch around the trailing edge at 0.9R disappeared rapidly at 65 deg. The RANS computations agree well with the experimental results qualitatively.

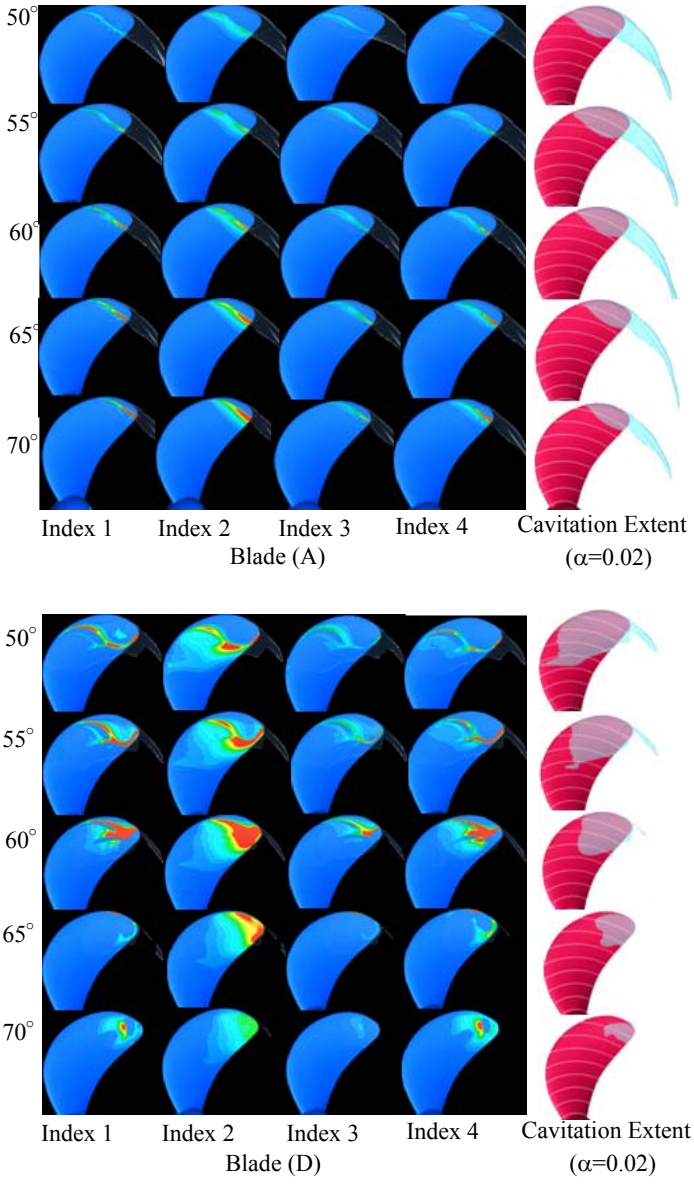

Fig. 38 Calculation Restults of Contours of Cavitation Erosion Indexes and Cavitation Extent

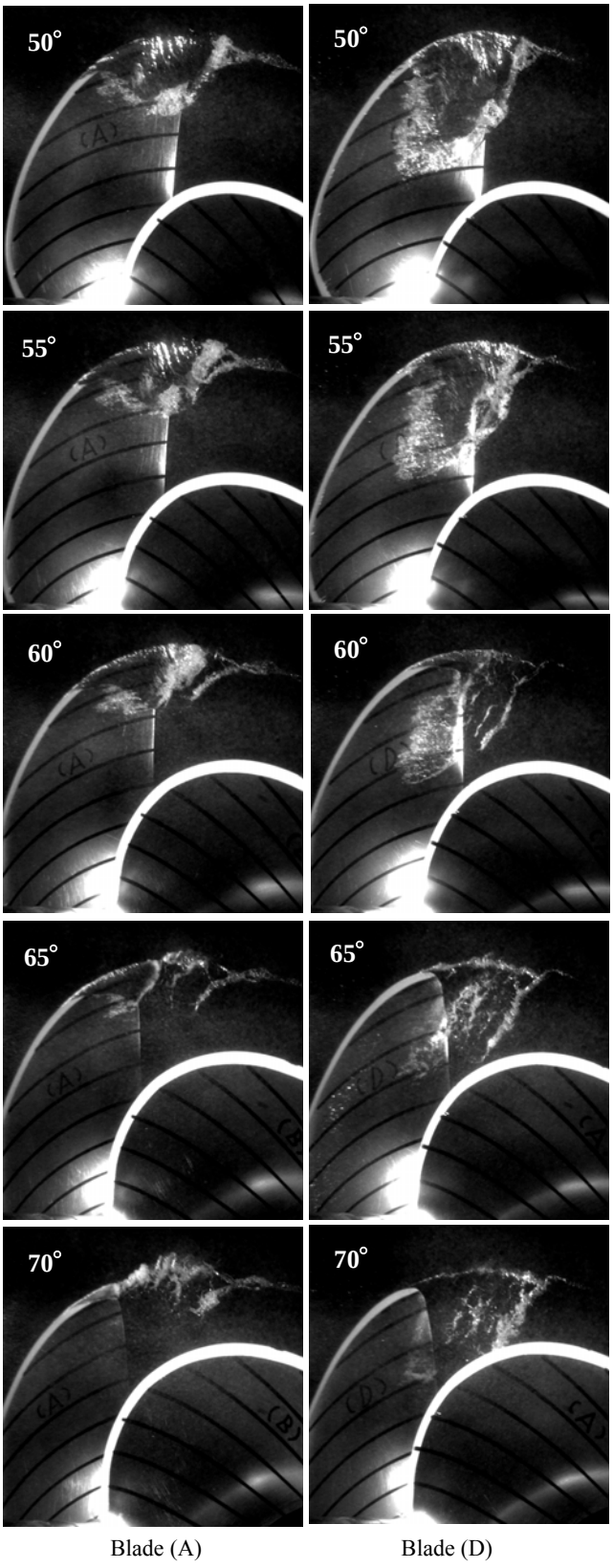

Fig.39 High Speed Video

CONCLUSIONS

This research found that velocity distribution in the boundary layer of the DTMB P4119 propeller and the wing tip vortex was obtained effectively by using the adaptive mesh refinement methodology. The SST k-ω model underestimated the boundary layer thickness and the k-ε model showed good agreement with experimental results. The SST k-ω model predicted the P.O.C. in good agreement with the experimental results and the k-ε model underestimated the propeller open efficiency.

The unsteady calculation of HSP was conducted and the unsteady non-cavitating calculation was validated. The computational results comparatively agreed with Hoshino's panel method. Pressure distribution at 0.9R trailing edge position was greatly different from the measurement results in full scale.

The computational cavitation shape of Seiun-Maru CP and HSP were compared with the experimental results, and agreement was obtained qualitatively in the distribution shape. The void fraction obtained by the calculation is comparatively low, and there is room for the accuracy improving. Room for argument remains to what value of cavity void ratio should be used for the comparison with the model experiment.

The model test of the propeller having various load distribution was conducted and the difference of the strength of tip vortex cavitation was observed. It was confirmed that RANS predicts the difference of the strength of tip vortex cavitation and the cavitation pattern like patch around the trailing edge.

Four simple indexes for the estimation of the erosion risk were applied to the analysis of the propeller operating in the wake flow. This research found that there is a possibility to estimate the difference of the erosion risk practicably by using simple index.

NOMENCLATURE

D	Propeller diameter
R	Propeller radius
J	Propeller advance ratio ($=V_A / nD$)
K_T	Thrust coefficient ($=T /\rho n^2D^4$)
K_Q	Torque coefficient ($=Q /\rho n^2D^5$)
η_o	Propeller efficiency ($=JK_T /2\pi K_Q$)
y^+	A non-dimensional wall distance for a wall-bounded flow ($=u^*y/\nu$)
y	Distance to the nearest wall
u*	Friction velocity
ν	Kinematic viscosity (m^2s^{-1})
σ_n	Cavitation number ($=2(P-P_V) /\rho n^2$)
C	Chord length
ρ	Density (kgm^{-3})
P	Pressure (Nm^{-2})
α	cavity void fraction
k	Kinetic turbulence energy
Cp	Pressure coefficient ($=P /\rho n^2D^2$)
x	Chordwise position from the leading edge
X	X is positive down stream,with its origin at the preopeller reference line
V	advance velocity
Vx-1	positive downstream (=VX/V-1)
Vr	positive outward (= VR/V)
Vt	positive is in direction of rotation (=VT/V)
Y/C	the distance normal from the wall normalize by chord

REFERENCES

Eckhardt, M. K. & Morgan, W.B.: A Propeller Design Method, Trans.SNAME. Vol. 63, 1955

Gindroz, B.,Hoshino, T. & Pylkkanen, V.: Propeller RANS/Panel Method Workshop,22nd ITTC Propulsion Committee Propeller RANS/Panel Method Workshop, Grenoble, Apr.1998.

Hasuike, N., Yamasaki, S. & Ando, J.: Prediction of Cavitation on Marine Propeller Using Generally Applicable Computation Fluid Dynamics, Proc. of 13th Symposium for Cavitation, Sapporo, Japan, 2006

Hasuike, N. & Yamasaki, S.: Anti-Singing Edge Effect on Propeller Open Characteristics, SNAME Propellers and Shafting 2006, Virginia, U.S.A. , 2006

Hasuike, N., Yamasaki, S. & Ando, J.: Prediction of Cavitation on Marine Propeller Using Generally Applicable Computation Fluid Dynamics, Proc. of 14th Symposium for Cavitation(2nd Report), Sendai, Japan, 2009

Hatano, S., Minakata, J. & Yamasaki, S: The Estimation of the Performance Characteristics of the Propeller by the Lifting Line and Lifting Surface Theory, Trans. of The West-Japan Society of Naval Architects, No. 49, 1975, pp.177-220

Holden, K. & Kvinge, T.: On Application of Skew Propellers to Increase Propulsion Efficiency, Proc. of 5th Lips Symposium, 1983, pp.4.3-4.19

Hoshino,T. :Experimental Data For Unsteady Panel Calculations And Comparison (Seiun-Maru HSP), Proceedings of Propeller RANS/Panel Method Workshop, 22nd ITTC Propulsion Committee, Grenoble, Apr.1998.

Jessup, S.D.:Experimental Data For RANS Calculations and Comparisons(DTMB P4119), 22nd ITTC Propulsion Committee Propeller RANS/Panel Method Workshop, Grenoble, Apr.1998.

Johnsson, C.-A.: Propeller Parameter Studies, Noise Sources in Ships: I Propellers, Nordforsk, Miljovardsserien, 1981, pp H1-H29

Kakugawa, A. & Takei, Y.: Measurement of Boundary Layer on a Propeller Blade Using LDV Technique, Journal of the Kansai Society of Naval Architects , Japan, No.203, 1986, pp.21-26

Kawamura, T. & Kiyokawa, T.: Numerical Prediction of Hull Surface Pressure Fluctuation due to Propeller Cavitation, Proc. of Conference Proceedings the Japan Society of Naval Architects and Ocean Engineers, Vol. 6, 2006, pp. 213-216

Kudo, T., Ukon, Y., Kurobe, Y.,Tanibayashi, H.: Measurement of shape of cavity on a model propeller blade, Journal of the Society of Naval Architects of Japan,

Vol.166, 1989, pp.93-103,

Kurobe, Y., Ukon, Y., Koyama, K., Makino, M.: Measurement of Cavity Volume and Pressure Fluctuations on a Model of the Traininng Ship "Seiun-Maru" with Reference to Full Scale Measurement, Rep.Ship Research Institue, Vol.20, No.6, 1983

Lerbs, H. W.: Moderately Loaded Propellers with a Finite Number of Blades and Arbitrary Distribution of Circulation, Trans. SNAME, Vol.60, 1952, pp.73-117

Moriya, T.: Introduction to Aerodynamics', Tokyo, 1959, Baifukan

Nohmi, M., Iga, Y., & Ikohagi, T.: Numerical Prediction Method of Cavitation Erosion, Conference Proceeding of Turbomachinery Societh of Japan, vol.59, 2008, pp. 49-54.

Okuda, K. & Ikohagi, T.: Numerical Simulation of Collapsing Behavior of Bubble Clouds, Transactions of the Japan Society of Mechanical Engineers.B, vol.62, 1996, pp.3792-3797

Salvatore, F.,Streckwall, H.,Terwisga, T.: Propeller Cavitation Modelling by CFD Results from the VIRTUE 2008 Rome Workshop',Proc. Of 1st international Symposium on Marine Propulsors smp'09, Trondheim, Norway, 2009

Singhal, A.K., Athavale,M.M., Li, H.Y., Jiang, Y.: Mathematical Basis and Validation of the full Cavitation model, Journal of Fluids Engineering, vol.124, 2002, pp.617-624

Sugai, K.: Proceedings of The 2nd Symposium on Marine Propellers, The Society of Naval Architects of Japan, Tokyo, Japan, 1971

Takahashi, H.: A Prevention from Face Cavitation by Varying the Form of Blade Sections of a Screw Propeller, Report of Transportation Technical Research Institute, No. 38, 1959

Ukon, Y. & Takei, Y.: An Investigation of the Effects of Blade Profile on Cavitation Erosion of Marine Propellers, Trans. of the West-Japan Society of Naval Architects, No.61, 1981, pp.81-93

Ukon, Y., et al.: Measurement of Pressure Distribution on a Full Scale Propeller -Measurement on a Conventional Propeller-, Journal of the Society of Naval Architects of Japan, Vol.168, Dec. 1990, pp.65-75.

Ukon, Y., et al.: Measurement of Pressure Distribution on a Full Scale Propeller -Measurement on a Highly Skewed Propeller-, Journal of the Society of Naval Architects of Japan, Vol.170, Dec. 1991, pp.111-123.

Ukon, Y., Kudo, T., Yuasa, H. & Kamiirisa, H.: Measurement of Pressure Distribution on Full Scale Propellers, Proceedings of the Propellers/Shafting '91 Symposium, the Society of Naval Architects and Marine Engineers, Virginia Beach, Sep. 1991.

Yamasaki, S.: A Numerical Method for Non-Linear Steady Propeller Lifting Surface and Its Application for Highly Skewed Propeller Design, Trans. of the West-Japan Society of Naval Architects, Vol. 62, 1981, pp. 47-68.

Yamasaki, S. & Okazaki, A.: Cavitation Test on a Straight Leading Edge Propeller and a Tip Rake Propeller, Journal of the Japan Society of Naval Architects and Ocean Engineers, Vol. 2, pp. 271-277.

Yamasaki, S., Okazaki, A., Ukon, Y. & Kawanami, Y.: Cavitation Test of a Propeller Having Blades Designed by Various Load Distributions near the Blade Tips 1st Report: Modification of Cavitation Simulation by using Propeller Lifting Surface Calculation, Proc. of Conference Proceedings the Japan Society of Naval Architects and Ocean Engineers, Vol. 6, 2008, pp. 197-200.

Yamasaki, S., Okazaki, A., Ukon, Y. & Kawanami, Y.: Cavitation Test of a Propeller Having Blades Designed by Various Load Distributions near the Blade Tips 2nd Report: Modification of Cavitation Simulation by using Propeller Lifting Surface Calculation, Proc. of Conference Proceedings the Japan Society of Naval Architects and Ocean Engineers, Vol. 6, 2008, pp. 201-204.

Yamasaki, S., Okazaki1, A., Hasuike, N. , Kawanami, Y. & Ukon, Y.: Numerical and Experimental Investigation into Cavitation of Propellers Having Blades Designed by Various Load Distributions near the Blade Tips, Proc. Of 1st international Symposium on Marine Propulsors smp'09, Trondheim, Norway, 2009